*Laser and Particle Beams* (1989), *vol.* 7, *part* 2, *pp.* 333–344
*Printed in Northern Ireland*



# Analysis, design and construction of copper vapor laser system

**By STEFANO CAVALIERI, ROBERTO PINI, RENZO SALIMBENI, UMBERTO VANNI, MATTEO VANNINI**
Instituto di Elettronica Quantistica del C.N.R., Via Panciatichi 56/30, 50127 Firenze, Italy.

**By PIO BURLAMACCHI**
Universita' di Cagliari, Dipartimento di Fisica Via Ospedale, 72-09124 Cagliari, Italy

**By LORENZO FINI**
Universita' di Firenze, Dipartimento di Fisica, Largo E. Fermi 2, 50125 Firenze, Italy

(Received 12 July 1988)

In this work construction characteristics and performance of a small scale self-heating copper vapor laser are presented. Analytical design of the thermal isolator is reported in some detail. Particular attention has been given to the knowledge of power deposition in the discharge to evaluate the component losses. In the optimized conditions the laser mean power is over 5 W, confirming the expected values. Details of the measurements on the system are also reported.

## 1. Introduction

Through studies by Gould (1965) seeking an efficient new laser media, an entire new class of potential laser materials was discovered: the neutral atomic metal vapors, excited to their own first levels.

In effect the intrinsic inefficiency of gas lasers (He–Ne, $Ar^+$) pushed many research efforts to the choice of active media not involving high energy levels of atoms or ions but in which the laser transition could happen in the lower lying states of a neutral atom. These media were called with the term 'cyclic laser' identifying the sequence of excitation, laser transition and collisional relaxation processes in cascade. Typical examples of this class of lasers are metal vapors such as copper or gold. The success of the Gould's proposal started a great deal of studies and technological developments mainly determined by the strategic interest connected to isotope separation programs for the assessment of the technology to up scale the output average power to several tens of watts (Isaev *et al.* 1972, I. Smilanski *et al.* 1979). Along one of these programs, technological achievements developed by Anderson *et al.* (1981) led to more reliable and powerful systems combining effectively high average power in a visible laser emission ready for many applications. However, in spite of the relatively long development time, the recognition of the limits in performance of present devices left room for research aimed at a simplified operation using metal halides (Astadjov *et al.* 1984) or sputtering produced metal vapor for room temperature operation. Also, worthy of note, is the work done in Oxford to increase reliability and possibly to extend in other parts of the spectrum the number of lines with an efficient emission (R. R. Lewis & C. E. Webb 1985).

In this article a description of the analysis of the design criteria employed in the construction of a laboratory prototype will be given. Lasing emission characteristics of

0263-0364/89/0702-0333$05.00

the prototype using copper vapor as an active medium will be presented together with scaling up capabilities of the design.

## 2. Kinetics and spectroscopy

Selection rules provide, for copper atoms, a suitable upper level ($^2$P) dipole connection to the ground state ($^2$S) while the lower level of the transition being at $^2$D state remains metastable. Transitions $^2P_{\frac{3}{2}} \rightarrow {}^2D_{\frac{5}{2}}$ and $^2P_{\frac{1}{2}} \rightarrow {}^2D_{\frac{3}{2}}$ determine two characteristic lines 5105·54 Å and 5782·13 Å respectively. During the discharge kinetic reactions take place providing a set of excitation paths:

$$Cu + e \rightarrow Cu^{**} + e$$

$$Cu + Ne^* \rightarrow Cu^{**} + Ne + E$$

$$Cu^+ e \rightarrow Cu^{**} + e + E$$

and a set of deactivation paths to the ground state:

$$Cu^* + Ne \rightarrow Cu + Ne$$

$$Cu^* + \text{wall} \rightarrow Cu$$

where Cu* and Cu** are the $^2D$ and $^2P$ respectively. These reactions are determined by a variety of processes such as excitation, recombinations, charge exchange reactions, Penning reactions, collisions with cell walls and neon. Modeling of the kinetics (M. J. Kushner 1981) has resulted in some important insights into the optimum operating regime. This can be schematically described as follows:

(1) Electron temperature distribution peaking at $5 \div 6$ eV
(2) Copper temperature in the range $1700 \div 2000$°K

Most of the electrical and design parameters arise from these requirements as will be described later on in some details.

## 3. Discharge excitation

In effect, in the design of the excitation system, the electron energy requirements suggest the so called $E/p$ factor to be in the order of $20 \div 50$ kV/cm bar which typically means discharge voltage of $20 \div 30$ kV per meter of length at a pressure of tens to hundreds of mbar. The buffer gas pressure is involved in many ways with several processes and parameters such as excitation and deactivation, breakdown voltage, impedance and power coupling to the discharge, electron temperature and density. So the above mentioned pressure range is a compromise to meet different demands. Typical self-terminating lasers require usually limited pulse durations in order to efficiently populate the upper level; in this kind of laser a duration of less than 50 nsec is usual. Saturation of population inversion occurring for a few hundred Amperes of peak discharge current implies then the use of capacitors of a few nF. The so called "energy transfer scheme" shown in figure 1 is employed to achieve fast discharge, relaxing the operating conditions of critical components such as the ceramic thyratrons employed as high repetition frequency switches. Table 1 summarizes typical values of the electrical parameters of the excitation circuit. In this operating regime, lasing can be easily obtained if a copper atom density of $0{\cdot}5 \div 1 \times 10^{15}$ cm$^{-3}$ is somehow provided in the discharge volume. This figure corresponds to a temperature in the range $1700 \div 2000$°K if metallic copper is used or $800 \div 900$°K if copper halides are used. In this work, design criteria will be presented for metallic copper.

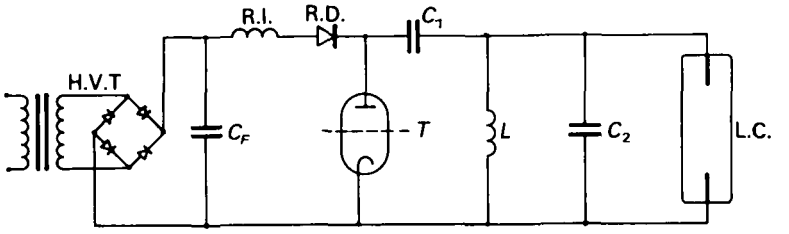


FIGURE 1. Energy transfer scheme of the excitation circuit H. V. T. High voltage transformer $C_F$ Supply filter capacitor, R. I. Resonance inductance, R. D. Resonant circuit diode, $C_1$ Storage capacitor, L Ground inducance, $C_2$ Peaking capacitor, L. C. Laser chamber.

| | |
|---|---|
| $C_1$ | 4 nF |
| $C_1$ Charge voltage | 10 kV |
| Thyratron peak current | 720 A |
| $C_2$ | 2 nF |
| Peak discharge voltage | 8.5 kV |
| Current discharge | 500 A |

TABLE 1. Electrical parameters in a typical operating condition.

## 4. Self-heating design

The proposal of this concept by Isaev *et al.* (1972) is based on the very simple recognition that, as long as a thermal isolation is provided, the power to have the required temperature can be given by electrical discharge at a suitable repetition rate. Then the electrical discharge provides both laser pumping and thermal heating. In effect most of the energy of the discharge is channeled through atom-atom and atom wall collisions to the gas and the wall itself rising their temperatures.

If $f$ is the repetition frequency, $C_1$ is the storage capacitor, $V$ is the charging voltage and $\delta$ is the fraction of the discharge energy transformed in thermal energy, the power:

$$P = \tfrac{1}{2} f C_1^2 \delta \tag{1}$$

will balance the heat waste determining a stationary solution inside the laser cell; to reduce this loss a suitable thickness of very low conductivity thermal isolation is provided around the discharge volume.

To know the power required for a given temperature we have evaluated the thermal dissipation in the approximation of infinite cylinder and considering as the main isolating material a low density alumina cylinder. In this condition the flow of heat per unit length is:

$$W = -2\pi r K \, dT/dr \tag{2}$$

where $r$ is the radial coordinate, $K$ the thermal conductivity and $T$ the temperature distribution. (In this geometry $T$ is only a function of $r$). For our material (low density alumina fibers), we have:

$$K = \alpha T + \beta \tag{3}$$

where $\alpha = 1{\cdot}29 \times 10^{-4}\,\mathrm{W\,°K^{-2}/m}$ and $\beta = 2{\cdot}05 \times 10^{-2}\,\mathrm{W\,°K^{-1}/m}$.

In our stationary condition $T(r)$ is given by the solution of:

$$d/dr(rK\,dT/dr) = 0 \tag{4}$$

with the boundary conditions $T(a) = T_2$ and $T(b) = T_1$.

The solution of equation (3) gives the following expression of $W$:

$$W = 2\pi(\alpha(T_2^2 - T_1^2) + 2\beta(T_2 - T_1))/(2 \ln (b/a)). \quad (5)$$

In this design $b = 6{\cdot}6$ cm, $a = 1{\cdot}3$ cm, $T_1 = 300$°K.

Power losses due to thermal conduction at both ends of the cylindrical cell have been evaluated in a constant K approximation: assuming a hemispherical model for the thermal isolation at the extremes and considering a reasonable average value of K, a comparison of the losses around the cylinder and the losses out of the two hemispherical ends give the ratio:

$$W_{sph}/W_{cyl} = 2ab \ln (b/a)/l(b - a)$$

which, in our case, has a value of 15%, being $l = 35$ cm the cylinder length.

Blackbody emission theory gives an estimate of the thermal irradiation through the ends:

$$W = 2S\varepsilon\sigma T^4$$

in which: $\varepsilon$ is the alumina emissivity, $\sigma$ is the Stefan-Boltzmann constant, and the irradiating surface has been approximated as the aperture of the hollow electrode.

## 5. Construction characteristics

Relying on the previous design considerations a metal vapor laser prototype has been constructed. Size choice has been driven mostly by the opportunity of a small device delaying a scaling-up process to a further extension of the research program. For this reason a compact laser cell has been devised with an active length of 38 cm, in which an input power in the order of 0·5 kW would be enough to provide optimum temperature in the laser cell. With a value of the efficiency around 1% (a usual good value) we can expect an output around 5 watt. Details of the design are shown in figure 2. The discharge cell is an alumina tube with inner diameter of 20 mm, outer diameter

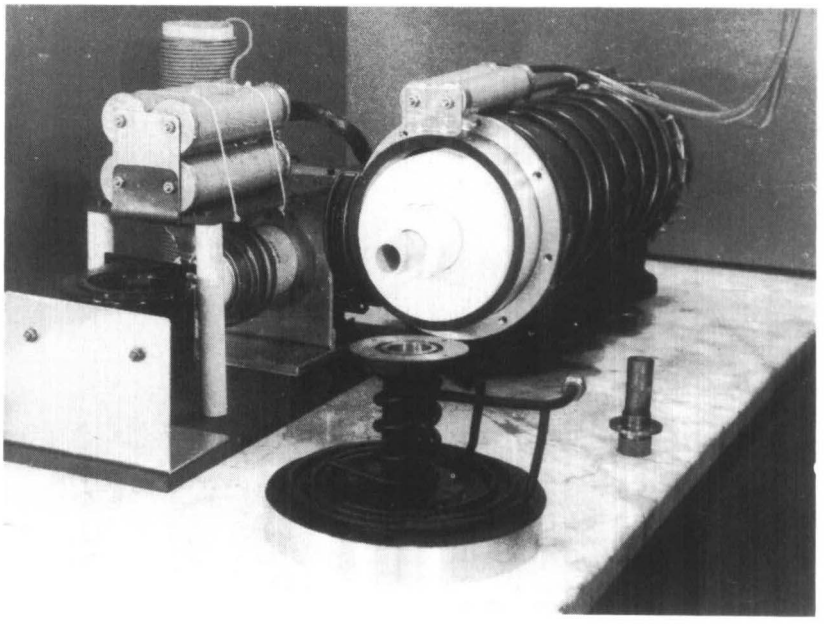

FIGURE 2. Exploded view of the laser chamber and part of the excitation circuit.

of 25 mm and a length of 50 cm. Choice of high purity alumina is forced by the operating temperature; an alternative could be zirconia tubes. The alumina tube is surrounded by a cylindrical thermal isolator of about 50 mm radial thickness. The isolating material is required to have analogous chemical properties of the laser channel; so alumina is a good material because of its wide range of thermal conductivity depending on the average density. Here a low density alumina material whose conductivity characteristics have previously been reported in (3), has been employed. Due to the low steady state temperature at the outer surface of the isolator, a Pyrex tube has been employed to contain the isolator and to provide a vacuum seal to the entire structure. Aluminum flanges are located at the extremes of the Pyrex tube to complete the vacuum seal and to support the two hollow molybdenum electrodes long enough to penetrate into the inner alumina tube for 6 cm.

Two window holders are mounted on the external surface of the flanges, by means of a 10-cm long neck to minimize dust or vapor deposition on the flat glass windows which have been slightly tilted to avoid back reflections into the laser channel. Gas inlet and outlet are provided at the holders' necks. A copper foil wrapped around the outer surface of the Pyrex tube and tightly coupled to one of the metal flanges covers 40 cm of the tube length providing a coaxial discharge current return for minimum inductance. Fluid cooling has been conservatively provided at the metal flanges (copper tubing for water circulation on both neck and surface) while, due to the limited value of the input power, air convection cooling has been successfully tested.

The excitation circuit is schematically shown in figure 1. The energy storage capacitor $C_1$ is composed of a set of mica capacitors of 1 nF each for minimum losses and reliable high frequency operation. $C_1$ is resonantly charged in about 300 $\mu$s through a suitable choke and a high voltage diode doubling the voltage of the power supply filter capacitor $C_F$. An air cooled ceramic thyratron, EEV model 1535A, controls the discharge rate of $C_1$ over $C_2$ which acts as a peaking capacitor and is a set of mica capacitors of 0.5 nF each. Due to the relatively low power requirements of this laser design, voltage and peak current in the thyratron have been kept at confidently low levels of $8 \div 10$ kV and $500 \div 700$ A respectively. Pulse repetition rate has been consequently set in the range of $5 \div 10$ kHz to supply an average power up to 1·5 kW. In effect, as will be described later, the power consumption of the power supply is modified by both energy exchange between the capacitive and inductive reactances and by the energy losses in critical components such as resonant choke ferrite core and ceramic thyratron.

## 6. Power deposition

When operation of the device was started in one typical condition, electrical discharge parameters and temperature of the inner tube were monitored to evaluate power deposition in the discharge and the temperature evolution. The gas column is contained inside the inner alumina tube in the design geometry of this prototype. The analytical evaluation of the overall power required to maintain a desired temperature in this design is presented in figure 3. Two main contributions are considered: 1) overall heat conduction; 2) thermal irradiation through the tube ends. As can be seen, the design parameters choice led to a power expense limited to 700 W, to obtain the operating temperature of copper or gold. Temporal behavior of voltage and current discharge as observed at the thyratron anode cup and at the laser cell cathode, are shown in figures 4a and 4b respectively. Their integration gives an experimental

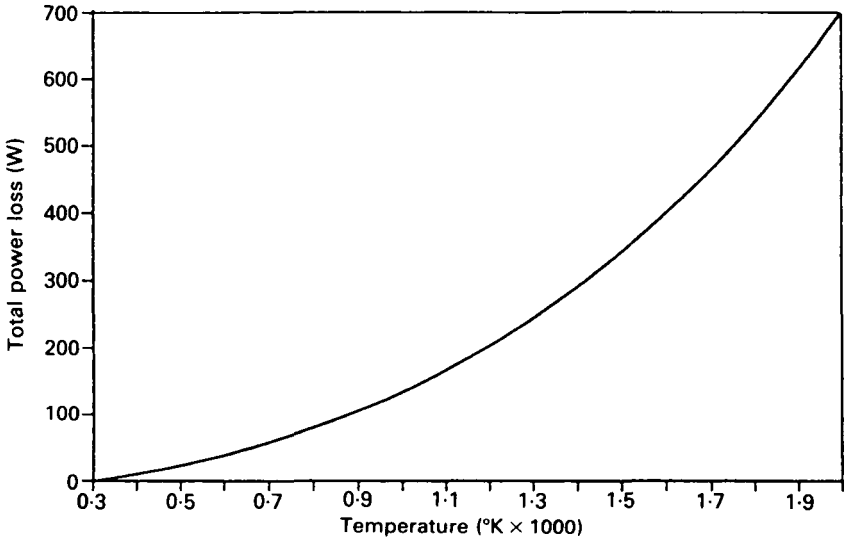


FIGURE 3. Analytically estimated power loss of the laser chamber vs. temperature.

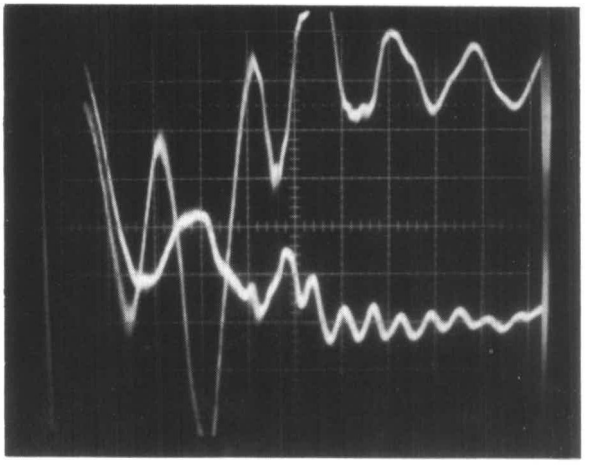

FIGURE 4a. Thyratron voltage and current: Higher swing, current pulse. Or. 50 nsec/div; ver. 2 kV/div and 100 A/div.

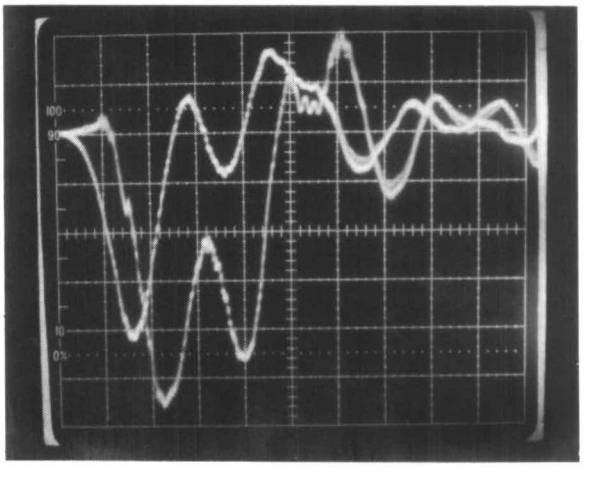

FIGURE 4b. Discharge voltage and current: Higher swing, current pulse. Or. 50 nsec/div; ver. 2 kV/div and 100 A/div.

| | |
|---|---|
| Power supply expense | 1200 W |
| H. V. transformer loss | 200 W |
| Resonant inductance hysteresis loss | 180 W |
| Thyraton conduction loss | 220 W |
| Discharge power deposition | 580 W |
| Condensers loss | 20 W |

TABLE 2. Main components power distribution.

measure of the power loss in a critical component such as the ceramic thyratron and the effective power dissipation in the laser discharge. Table 2 summarizes the main contributions to the power losses measured in optimum lasing conditions. Temperature evolution and power supply expense during the heating time are shown in figure 5. The results confirm an effective power requirement in the order of 600 W for a steady temperature of 1820°K, as measured by an optical pyrometer. It has to be noted that a large fraction of the power supply expense is due to the H.V. transformer loss which could be minimized. A heavy balance is also due to lossy and saturated hysteresis of the ferrite core of the resonant choke. Less avoidable appears the switch loss in the thyratron which could be eventually minimized by means of a magnetic assist to delay the current onset. Also worthy of note is the negative voltage recharging of $C_1$ mainly due to the energy stored in the current transients through $L_{res}$ and the partial energy transfer to $C_2$ and to the discharge impedance. These effects result in an overdoubling of the power supply voltage in such a way that in typical conditions $C_F$ remains charged at 3·7 kV where $C_1$ is steadily charged at 10 kV.

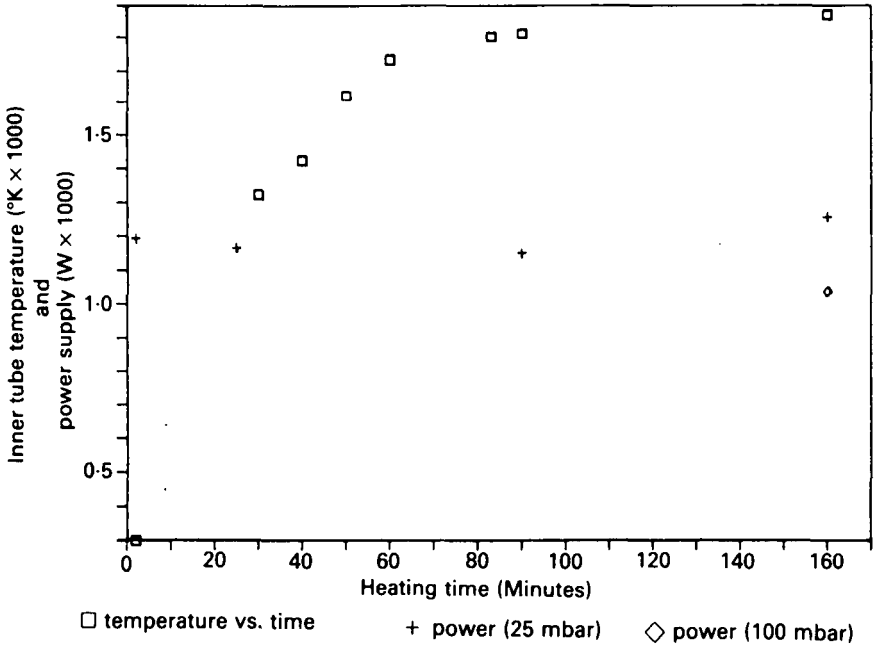


FIGURE 5. Temperature and power supply vs. time. The power supply is reported for two different values of Ne partial pressure.

## 7. Laser performance

An analysis of the spectral content of the fluorescence emitted by the gas column was employed to examine the rise of fluorescence on the laser transitions and the eventual presence of contaminants such as sodium which could worsen the laser performance. Figure 6 reports a fluorescence spectrum during the heating time of the device. As expected at high temperature, the two copper fluorescene lines become strong together with the characteristic lines of sodium, demonstrating that a higher purity of the inner alumina cylinder would probably be desirable. After approximately 40 minutes, lasing on the 510-nm line started, providing a standard optical resonator consisting of a flat aluminized mirror and an uncoated glass flat as the output coupler. Due to the lack of total reflectors with reflectivity higher than 90%, resonator optimization was limited to the choice of a roof prism and uncoated quartz flat. Optimization of the average power acting sequentially on different parameters is somewhat complicated by the overposition of effects of both power dissipation in the tube and the effective excitation process which unavoidably occurs with every parameter variation.

For this reason the following results cannot discriminate between contribution of different copper vapor pressures and different excitation rates, but pertain to the evaluation of the overall performance of the laser system described by the total laser output power. With these premises the following set of measurements have been performed:

a) At constant input power in the order of 1 kW, buffer gas pressure has been varied monitoring the long-term variations of the output power.

b) At optimum pressure laser performance at three different pulse rates has been monitored varying the storage capacitor $C_1$ for constant input power.

c) At optimum rate and pressure $C_1/C_2$ ratio has been varied to verify the energy transfer efficiency effects. Figure 7 and table 3 describe the general trends of the laser output dependence on the overmentioned parameters. For better comprehension of these results, a few comments are worth citing.

He, as buffer gas, requires pressure lower than 10 mbar, while Ne pressure can be raised to 100 mbr which, in this laser system, represents the optimum buffer gas

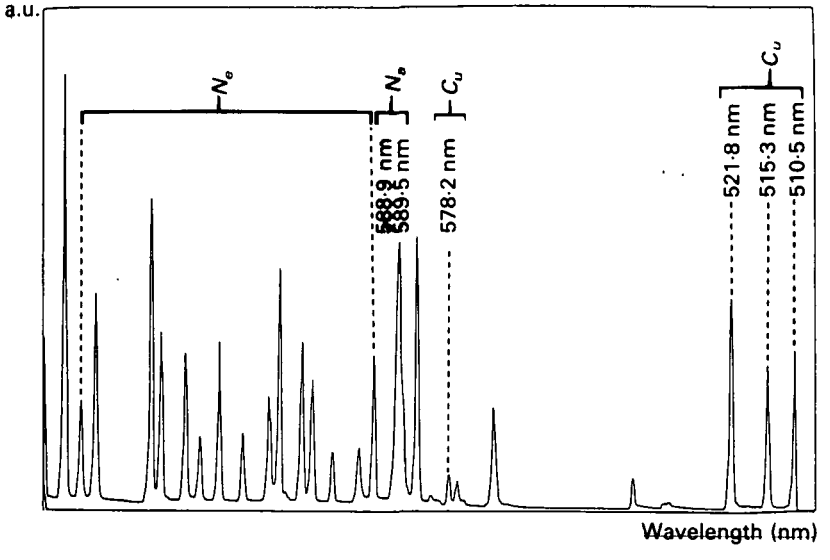


FIGURE 6. Fluorescence spectrum during heating time.

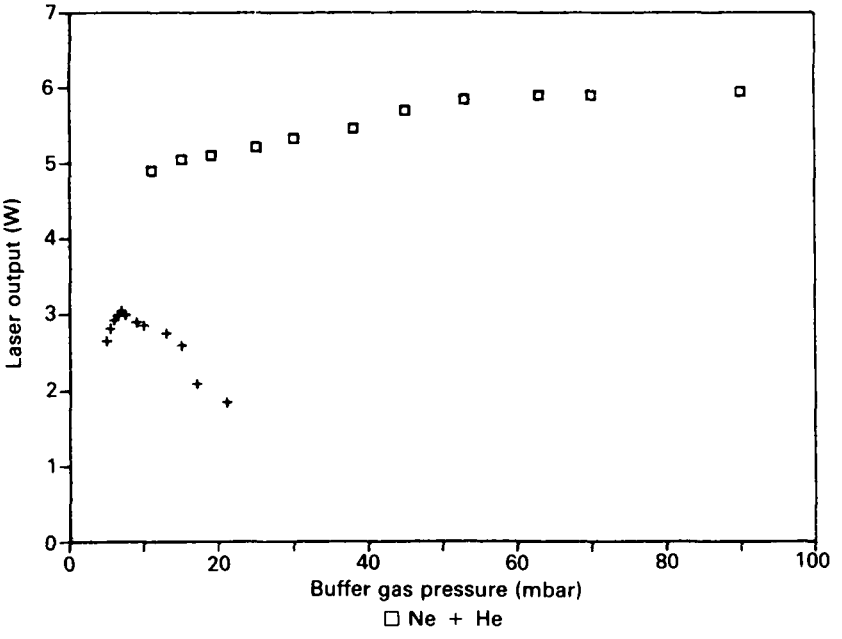


FIGURE 7. Laser power output vs. pressure of two different buffer gases (He, Ne).

pressure. As reported by O. R. Marasasov and St. Stoilov (1983), an even higher gas pressure could be employed, but here the relatively low discharge voltage results in a reduced power deposition and a worsening of the laser power. A noticeable improvement has been obtained lowering the gas recirculation flow to almost negligible values, denoting probably a maximum value for the vapor column length in static conditions.

As seen in table 2, in the range of variation of the parameters $C_1$, p.p.r. and $C_1/C_2$, the total laser output power results are quite constant, depending only on power deposition and consequently on tube temperature and copper atoms density. This dependence has been investigated setting the operating conditions of pressure (35 mbar Ne) and slow flow (<0·1 l/h) and raising $C_1$ charge voltage. While with a power supply expense of 1·2 kW the laser output reached a steady maximum of 5·6 W at 1820°K, increasing the power to 1·6 kW, allowing a higher temperature to be reached. During the new steady temperature approach a temporary maximum for the total laser output

| | | $C_2$(nF) | | | |
|---|---|---|---|---|---|
| | | 0·5 | 1·0 | 1·5 | $f$(kHz) |
| $C_1$(nF) | 4 | 4·7 | 5·4 | 5·3 | 5·00 |
| | 3 | 5·4 | 5·6 | 5·5 | 6·66 |
| | 2 | 5·4 | 5·6 | 5·0 | 10·00 |

TABLE 3. Laser power output (W) for various $C_1$, $C_2$ and repetition rate combinations at constant power supply expense.

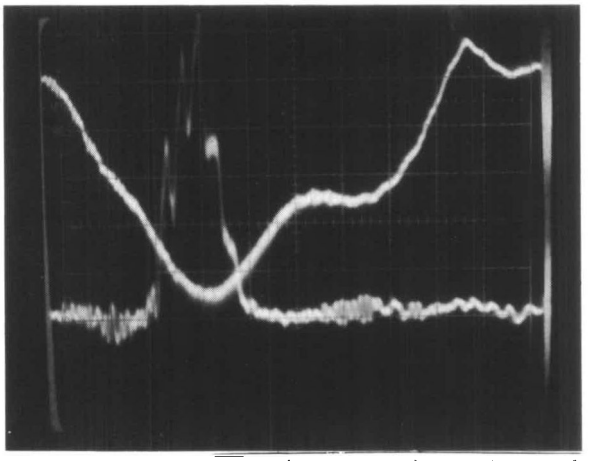

FIGURE 8a. Temporal behavior of 510 nm line (upper trace) superimposed on discharge current (lower trace): Ver. a.u. or. 20 nsec/div.

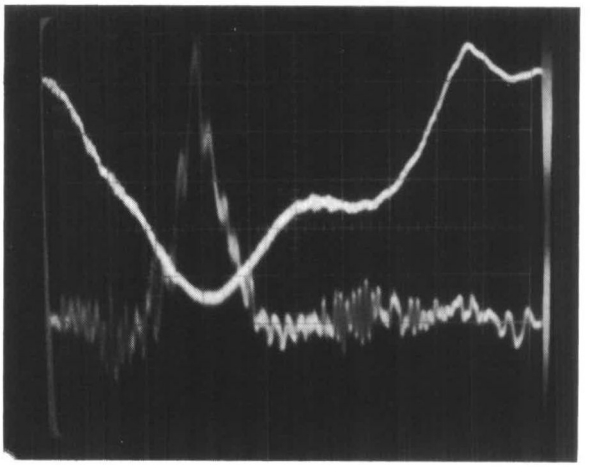

FIGURE 8b. Temporal behavior of 578 nm line (upper trace) superimposed on discharge current (lower trace): ver. a.u. or 20 nsec/div.

of 7 W was observed, but when the tube temperature overcome 1920°K the laser power level decreased showing a worsening of the overall performance. This observation set a limit to the operating temperature of the copper, but at the same time, demonstrates the possibility of this prototype to operate with a moderate amount of power at the temperature levels (1900 ÷ 2000°K) usually required to optimize the laser performance of gold vapors.

Temporal behavior of copper vapor laser emission on the two lines at 510 and 578 nm are reported in figure 8a and 8b respectively, in relationship with the gas discharge current pulse, to put in evidence the slight delay of the 578 nm line. A presentation of the total laser emission is given in figure 9 as the graphic output of DCS Tektronix digital camera coupled to a 500 MHz mod. 31101 oscilloscope, for a more reliable knowledge of the pulse details.

Table 4 summarizes the main parameters of the laser performance.

In conclusion, details of the design of a small scale copper vapor laser have been presented. The operation of a preliminary prototype confirms the expected power in

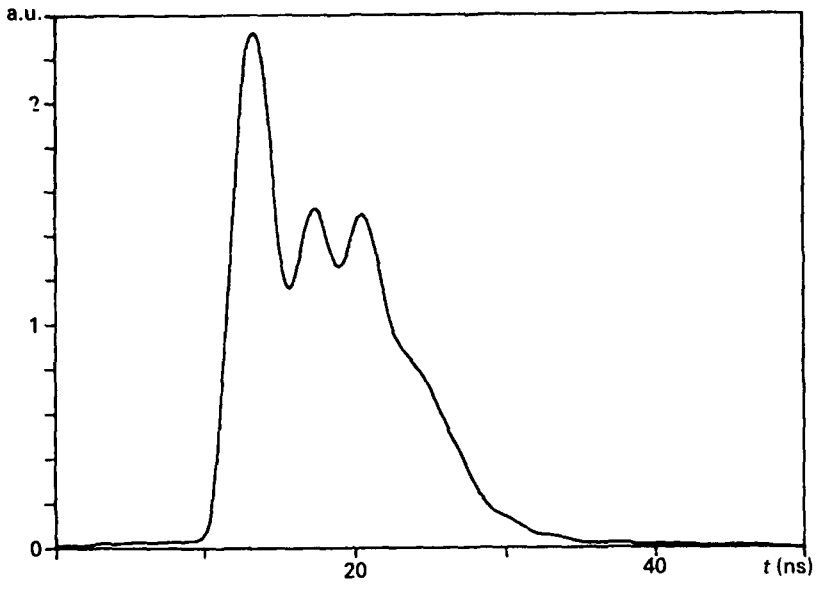


FIGURE 9. Temporal behavior of total laser power output.

| | |
|---|---|
| Beam diameter | 20 mm |
| Average power on both lines @ 1823 °K | 5·6 W |
| 510 nm energy @ 5 kHz | 0·65 mJ |
| 578 nm energy @ 5 kHz | 0·47 mJ |
| 510 nm peak power @ 5 kHz | 70 kW |
| 578 nm peak power @ 5 kHz | 65 kW |
| 510 nm pulsewidth FWHM | 9 ns |
| 578 nm pulsewidth FWHM | 7 ns |
| Energy extraction | $10^{-2}$ J/l |
| Overall efficiency | 0·46% |
| Discharge efficiency | ≈1% |

TABLE 4. Copper vapor laser output parameters.

the order of 5 W at an overall efficiency of 0·5% which represents a reasonable figure compared with similar size device performance. Future improvements in this research program will deal with power laser optimization to approach an effective 1% efficiency level. At the present energy extraction of $10^{-2}$ J/l, an adequate up-scaling of the discharge volume is also promising to enter the tens of watts power level with copper vapors. Finally, the present design is amenable to reach, with a moderate power expense operating temperatures also useful for gold vapor excitation.

## Acknowledgments

The authors acknowledge the financial support provided by the Strategic Project 'Optoelettronica' and the 'Progetto Finalizzato' 'Tecnologie ElettroOttiche' of the 'Consiglio Nazionale delle Ricerche' of Italy.

## REFERENCES

ANDERSON, R. S. *et al.* 1981 Dig. of Techn. Papers CLEO.
ASTADJOV, D. N. *et al.* 1984 *Opt. Comm.*, **51,** 85.
GOULD, G. 1965 *Appl. Optics Suppl.*, **2,** 59.
ISAEV, A. A. *et al.* 1972 *JEPT lett.*, **16,** 27.
ISAEV, A. A. *et al.* 1972a, *ZhETF Pis. Red.*, **16,** 40.
KUSHNER, M. J. 1981 *IEEE J. of Quant. Electr.*, **QE-17,** 1555.
LEWIS, R. R. & WEBB, C. E. 1985 Dig. of Techn. Papers CLEO.
MARASAVOV, O. R. & STOILOV, ST. 1983 *Opt. Comm.*, **46,** 221.
SMILANSKI, I. *et al.* 1979 *Opt. Comm.*, **30,** 70.